Supplementary Information (SI) for RSC Advances.
This journal is © The Royal Society of Chemistry 2025

Supporting Information

Synergistic activation of peroxymonosulfate by highly dispersed iron-based sulfur-nitrogen co-doped porous carbon for Bisphenol A removal: Mechanistic insights and selective oxidation

Yu Sun, Chuning Zhang, Yan Jia*, Yalei Zhang, Jianwei Fan

State Key Laboratory of Pollution Control and Resources Reuse, College of Environmental Science and Engineering, Shanghai Institute of Pollution Control and Ecological Security, Tongji University, Shanghai 200092, P.R. China

∗Corresponding Author

E-mail address: jiay@tongji.edu.cn (Yan Jia)

Texts

Tables

Figures

Text S1. Reagents and Chemicals.

Potassium monopersulfate triple salt (PMS, $KHSO_5 \cdot 0.5KHSO_4 \cdot 0.5K_2SO_4$, ≥ 99.5%), 1-allylthiourea, Iron nitrate nonahydrate ($Fe(NO_3)_3 \cdot 9H_2O$), bisphenol A (BPA), Rhodamine B (RhB), sulfamethoxazole (SMX), hydrochloric acid (HCl, 37 wt.%), sodium hydroxide (NaOH), sulfuric acid (H_2SO_4, ＞ 98.0%), methyl alcohol (MeOH), ethanol absolute (EtOH), acetonitrile (ACN), Formate, isopropyl alcohol (IPA), tert-butyl alcohol (TBA) and furfuryl alcohol (FFA) were purchased from Sinopharm Chemical Reagent Co., Ltd., China. Potassium thiocyanate (KSCN), p-Benzoquinone (q-BQ), Norfloxacin (OFL), 4-Chlorophenol (4-CP), Methyl Phenyl Sulfoxide (PMSO), 5,5-Dimethyl-1-pyrroline N-oxide (DMPO, ≥ 97 %), and 2,2,6,6-tetramethyl-4-piperidinol (TEMP, 99 %) were obtained from Aladdin Biochemical co., Ltd. (Shanghai, China). P-Chlorophenol (4-CP) was obtained from Shanghai Macklin Biochemical Co., Ltd. Benzoic acid (BA) and 4-nitrophenol (4-NP) was purchased from Shanghai Boer Chemical Reagent Co., Ltd. Silicon dioxide (SiO_2) powder (20 nm) was purchased from Jinan Zhiding Welding Material Co., Ltd. Except for the mobile phase, which is chromatographically pure, all chemicals are of analytical grade and used without any further purification. Deionized water (18.25 MΩ cm) was used in all experiments.

Text S2. Characterizations.

The morphology of elements on the surface of FeSNC was examined using Scanning Electron Microscope (SEM) (Zeiss Merlin Compact). Energy Dispersive X-ray Detector (EDX) was analyzed by EDAX Inc. GENESIS. The degree of graphitization and defects in FeSNC was observed by Raman spectroscopy (Horiba LabRAM HR Evolution). The specific surface area, pore volume, pore size distribution and N_2 adsorption-desorption isotherms were determined by Quantachrome Autosorb-IQ3 analyzer. The specific surface areas (S_{BET}) were calculated using Brunauer-Emmett-Teller (BET) equation, and the pore size distribution was calculated using the Barrett-Joyner-Halenda (BJH) model. X-Ray Diffraction (XRD) patterns were obtained using Bruker D8 Advance equipped with Cu Kα radiation (40kV, 40 mA). X-ray

Photoelectron Spectroscopy (XPS) analysis was carried out on a Thermo Scientific K-Alpha X-ray Photoelectron Spectrometer with Al Kα X-ray (hν = 1486.6 eV) radiation.

Text S3. Experimental details of the EPR analysis.

The common DMPO and TEMP were used as spin trapping agents. In the water-mediated system, DMPO was used to trap ·OH/SO_4·$^-$ and TEMP was used to trap $^1O_2$ produced in the reaction. In the methanol-mediated system, DMPO was used to trap O_2·$^-$ produced. The specific operating parameters were: center magnetic field of 3500.00 G, swept field width 100.0 G, power of 6.325 mW; microwave attenuation 15.0 dB resonant frequency 9.826386 GHz, swept field time 30.00 s, modulation amplitude 1.000 G, modulation frequency 100.00 kHz, and number of sweeps 3 times.

Text S4. Electrochemical test.

Using a standard three-electrode system, electrochemical experiments were performed on a CHI 660E electrochemical workstation. The working electrode was prepared as follows: 10.0 mg of FeSNC catalyst was weighed and mixed with 2.0 mL of ethanol and 0.25 mL of 5 wt.% Nafion solution (binder), and ultrasonication was carried out for 1 h to fully disperse the catalyst, and 20 μL of the dispersion was coated on a glassy carbon electrode, which was dried overnight in an oven at 60 ℃. A platinum sheet and a saturated silver chloride electrode were used as the counter electrode and reference electrode, respectively. The I-t curve of the catalyst was tested with 50 mM Na_2SO_4 as the electrolyte, and the applied voltage was -0.5 V. PMS and organic pollutants were added to the electrolyte solution at 100 s and 200 s, respectively, and the current changes were observed.

Table S1. HPLC conditions for organic contaminants

Organic pollutants	mobile phase (V/V)	flow rate ($mL \cdot min^{-1}$)	Wavelength (nm)
BPA	MeOH/UPW = 70/30	1.0	230
SMX	ACN/UPW = 30/70	1.0	265
OFL	ACN/1% Phosphoric acid = 15/85	1.0	288
4-CP	MeOH/UPW = 70/30	1.0	278
NB	ACN/UPW = 50/50	1.0	270
TC	MeOH/0.1% Phosphoric acid = 60/401.0	1.0	360
BA	MeOH/ 0.2 M ammonium acetate solution = 10/90	1.0	230

Table S2. Surface elemental content of FeSNC

Name	Atomic %	PP At. %
C1s	87.49	91.92
Fe2p	0.33	0.11
N1s	11.47	6.84
S2p	0.72	1.12

Table S3. BET specific surface area, pore volume and pore size of FeSNC, FeNC and SNC

catalyst	S_{BET} ($m^2 \cdot g^{-1}$)	pore volume ($cm^3 \cdot g^{-1}$)	Average pore size (nm)
FeSNC	349.1	0.618	7.93
FeNC	90.1	0.119	6.63
SNC	360.7	0.849	10.82

Table S4. Comparison of the catalytic activity of FeSNC with reported catalysts

Catalyst dosage (mg/L)	PMS (mM)	Pollutants (mg/L)	Removal Efficicy (%)	Reaction Time (min)	Ref.
FeSNC (0.1)	1.00	BPA (20)	100	3	This work
DPA-Fe_2O_3 (0.5)	3.25	BPA (15)	90	120	(1)
$Fe_{0.8}Co_{2.2}O_4$ (0.1)	0.33	BPA (20)	95	60	(2)
$CuFe_2O_4$ (0.4)	0.81	BPA (50)	95	60	(3)
GAC (1.0)	5.70	AO7 (20)	100	60	(4)
N-rGO (0.12)	0.8	BPA (88)	95	7	(5)
Ca-BSAC (0.1)	0.33	BPA (22.83)	100	30	(6)
FeCNx-700 (50)	0.15	BPA (0.088)	94	5	(7)
$FeCo_2S_4$-CN (20)	0.15	SMX (4.99)	91.9	15	(8)
3D γ-MnO_2@$ZnFe_2O_4$/rGO (0.1)	6.5	Phenol (20)	100	30	(9)
Co@N-C (0.1)	0.25	BPA (10)	100	10	(10)
FeOOH/Mt-TC-C (0.1)	1.00	BPA (20)	100	30	(11)
FeNP-N-C (0.15)	0.66	BPA (20)	100	30	(12)
Pd/g-C_3N_4 (0.1)	1.00	BPA (20)	60	91	(13)
Fe-NS@C (0.1）	1.00	BPA (20)	100	15	(14)
Fe-N-BC (0.2)	1.00	AO7 (20)	100	90	(15)
FeSA-N-C-20 (0.15)	0.65	BPA (20)	100	30	(16)
EC-700-W (0.2)	0.5	SDZ (10)	100	60	(17)
SA-Mn-NC (0.05)	1.0	BPA (20)	100	5	(18)
NGC700 (0.1)	0.65	BPA (20)	98	4	(19)

Table S5. Actual Fe content of FeSNC and FeNC

catalyst	Me (wt.%)
FeSNC	0.64
FeNC	4.81

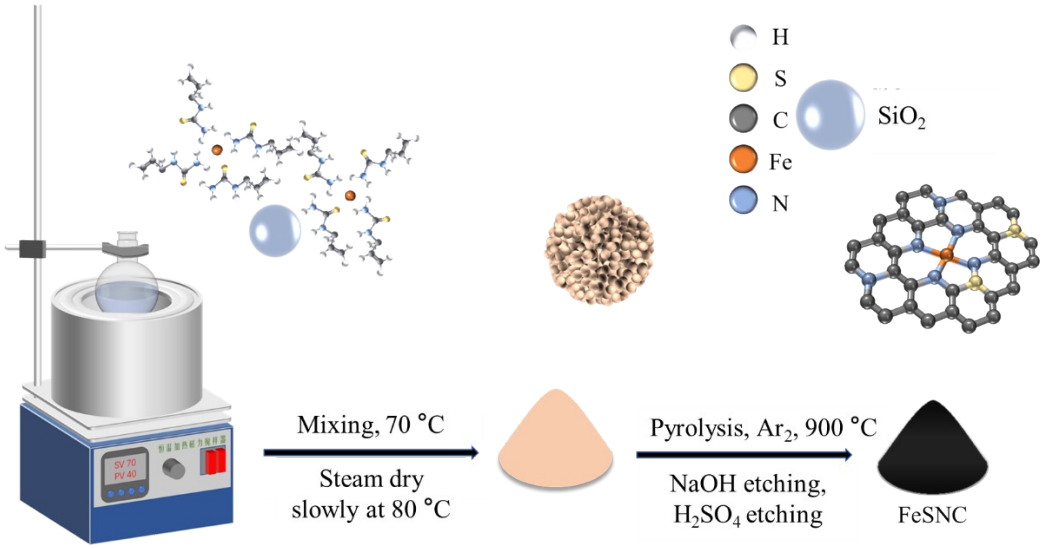

Fig. S1. Preparation of FeSNC catalyst

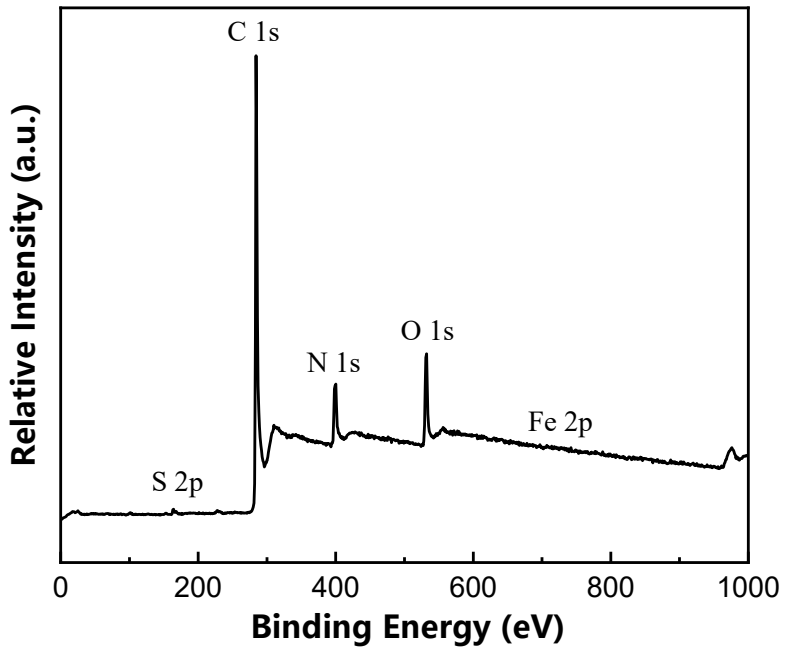

Fig. S2. XPS survey of FeSNC.

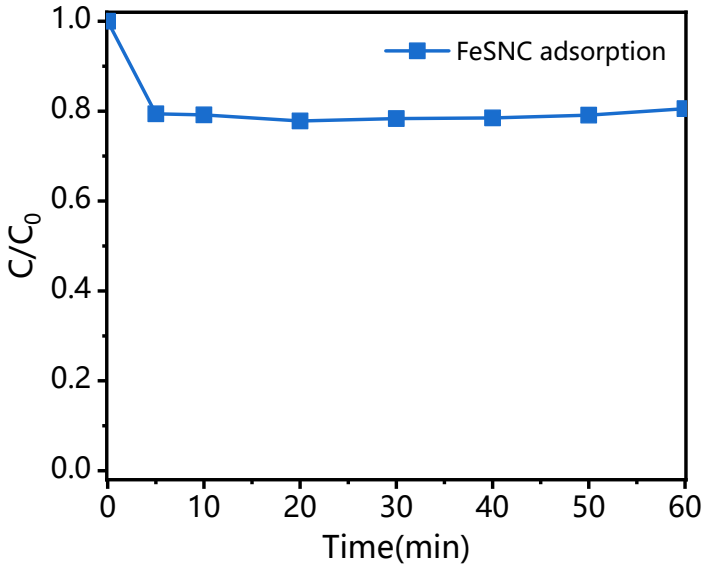

Fig. S3. Kinetic curves of BPA adsorption by FeSNC.

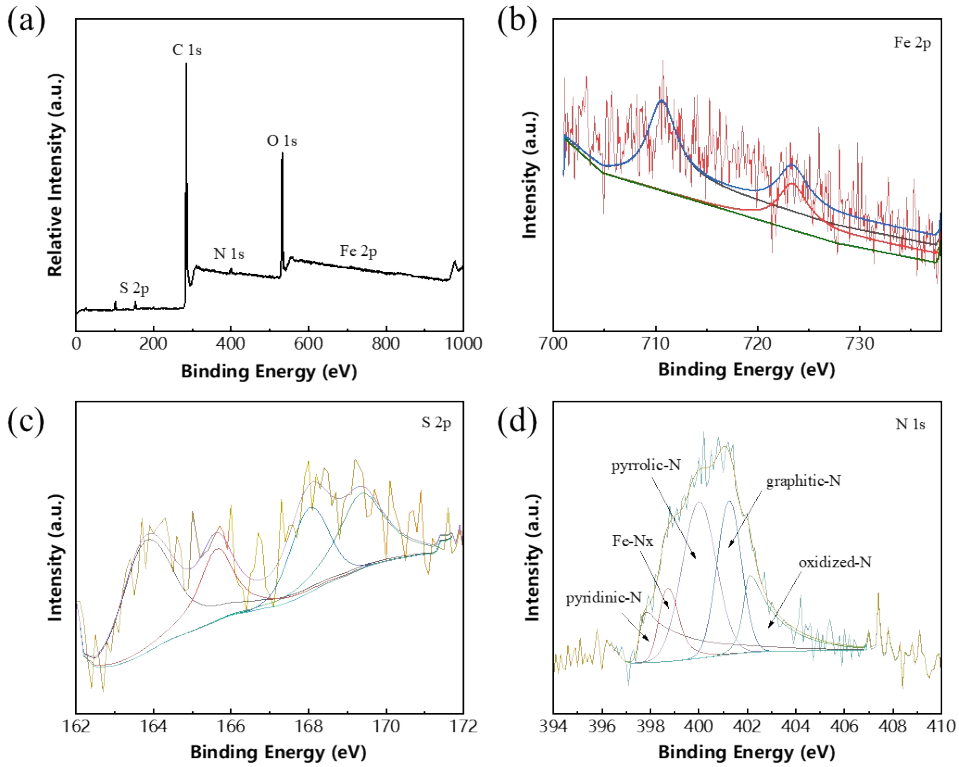

Fig. S4. (a) XPS survey of used FeSNC; High-resolution XPS spectrum of (b) Fe 2p, (c) S 2p and (d) N 1s of used FeSNC.

Reference

1. Oh WD, Lua SK, Dong Z, Lim TT. High surface area DPA-hematite for efficient detoxification of bisphenol A via peroxymonosulfate activation. Journal of Materials Chemistry A. 2014;2(38):15836-45.
2. Li X, Wang Z, Zhang B, Rykov AI, Ahmed MA, Wang J. FexCo3-xO4 nanocages derived from nanoscale metal-organic frameworks for removal of bisphenol A by activation of peroxymonosulfate. Applied Catalysis B: Environmental. 2016;181:788-99.
3. Xu Y, Ai J, Zhang H. The mechanism of degradation of bisphenol A using the magnetically separable CuFe2O4/peroxymonosulfate heterogeneous oxidation process. Journal of Hazardous Materials. 2016;309:87-96.
4. Zhang J, Shao X, Shi C, Yang S. Decolorization of Acid Orange 7 with peroxymonosulfate oxidation catalyzed by granular activated carbon. Chemical Engineering Journal. 2013;232:259-65.
5. Wang X, Tang P, Ding C, Cao X, Yuan S, Zuo X, et al. Simultaneous enhancement of adsorption and peroxymonosulfate activation of Nitrogen-doped reduced graphene oxide for bisphenol A removal. Journal of Environmental Chemical Engineering. 2017;5(5):4291-7.
6. Huang B-C, Huang G-X, Jiang J, Liu W-J, Yu H-Q. Carbon-Based Catalyst Synthesized and Immobilized under Calcium Salt Assistance To Boost Singlet Oxygen Evolution for Pollutant Degradation. ACS Applied Materials & Interfaces. 2019;11(46):43180-7.
7. Miao W, Liu Y, Wang D, Du N, Ye Z, Hou Y, et al. The role of Fe-Nx single-atom catalytic sites in peroxymonosulfate activation: Formation of surface-activated complex and non-radical pathways. Chemical Engineering Journal. 2021;423:130250.
8. Li Y, Li J, Pan Y, Xiong Z, Yao G, Xie R, et al. Peroxymonosulfate activation on FeCo2S4 modified g-C3N4 (FeCo2S4-CN): Mechanism of singlet oxygen evolution for nonradical efficient degradation of sulfamethoxazole. Chemical Engineering Journal. 2020;384:123361.
9. Mady AH, Baynosa ML, Tuma D, Shim J-J. Heterogeneous activation of peroxymonosulfate by a novel magnetic 3D γ-MnO2@ZnFe2O4/rGO nanohybrid as a robust catalyst for phenol degradation. Applied Catalysis B: Environmental. 2019;244:946-56.
10. Li H, Tian J, Zhu Z, Cui F, Zhu Y-A, Duan X, et al. Magnetic nitrogen-doped nanocarbons for enhanced metal-free catalytic oxidation: Integrated experimental and theoretical investigations for mechanism and application. Chemical Engineering Journal. 2018;354:507-16.
11. Yang S, Duan X, Liu J, Wu P, Li C, Dong X, et al. Efficient peroxymonosulfate activation and bisphenol A degradation derived from mineral-carbon materials: Key role of double mineral-templates. Applied Catalysis B: Environmental. 2020;267:118701.
12. Li Y, Yang T, Qiu S, Lin W, Yan J, Fan S, et al. Uniform N-coordinated single-

atomic iron sites dispersed in porous carbon framework to activate PMS for efficient BPA degradation via high-valent iron-oxo species. Chemical Engineering Journal. 2020;389.
13. Wang Y, Cao D, Liu M, Zhao X. Insights into heterogeneous catalytic activation of peroxymonosulfate by Pd/g-C₃N₄: The role of superoxide radical and singlet oxygen. Catalysis Communications. 2017;102:85-8.
14. Chen W, Lei L, Zhu K, He D, He H, Li X, et al. Peroxymonosulfate activation by Fe-N-S co-doped tremella-like carbocatalyst for degradation of bisphenol A: Synergistic effect of pyridine N, Fe-Nx, thiophene S. Journal of Environmental Sciences. 2023;129:213-28.
15. Li X, Jia Y, Zhou M, Su X, Sun J. High-efficiency degradation of organic pollutants with Fe, N co-doped biochar catalysts via persulfate activation. Journal of Hazardous Materials. 2020;397:122764.
16. Li Y, Yang T, Qiu S, Lin W, Yan J, Fan S, et al. Uniform N-coordinated single-atomic iron sites dispersed in porous carbon framework to activate PMS for efficient BPA degradation via high-valent iron-oxo species. Chemical Engineering Journal. 2020;389:124382.
17. Niu L, Lei Q, Zhao T, Tang Z, Cai Y, Hou D, et al. In situ N-doping engineered biochar catalysts for oxidation degradation of sulfadiazine via nonradical pathways: Singlet oxygen and electron transfer. Science of The Total Environment. 2024;939:173206.
18. Jia Y, Chen Y, Xue Y, Fan J. Efficient activation of peroxymonosulfate by Mn single-atom: Critical role of Mn-N4 coordination for generating singlet oxygen. Separation and Purification Technology. 2024;335.
19. Luo R, Li M, Wang C, Zhang M, Nasir Khan MA, Sun X, et al. Singlet oxygen-dominated non-radical oxidation process for efficient degradation of bisphenol A under high salinity condition. Water Research. 2019;148:416-24.